separations

MDPI

*Article*

# Adsorption Properties and Mechanism of Copper Ions from Wastewater by *Lessonia nigrescens* and *Lessonia nigrescens* Residue

**Haoran Chen [1], Rui Zhang [1,*], Xiaohan Qu [1], Yuan Yuan [2], Bo Zhu [3], Shichao Zhao [1] and Tengyao Jiang [4,5,*]**

[1] College of Materials & Environmental Engineering, Hangzhou Dianzi University, Hangzhou 310018, China; zhaoshichao@hdu.edu.cn (S.Z.)
[2] Marine Agriculture Research Center, Tobacco Research Institute of Chinese Academy of Agricultural Science, Qingdao 266101, China; yuanyuan03@caas.cn
[3] Ministry of Agriculture Key Laboratory of Seaweed Fertilizers, Qingdao Brightmoon Seaweed Group Co., Ltd., Qingdao 266440, China
[4] School of Environmental Science and Engineering, Nanjing Tech University, Nanjing 211816, China
[5] SMARL Lab, Innovation Center of Yangtze River Delta, Zhejiang University, Jiaxing 314100, China
* Correspondence: rui.zhang@hdu.edu.cn (R.Z.); jiangty@njtech.edu.cn (T.J.)

**Abstract:** Given the advantages of readily availability, low cost, convenient operation, and large adsorption capacity, brown seaweed has been studied extensively as a biosorbent for heavy metal remediation from aqueous media. Herein, raw *Lessonia nigrescens* and brown seaweed residue, a waste product from the manufacturing of alginate from *L. nigrescens*, were employed as low-cost and renewable adsorption materials for effective copper removal in wastewater streams. The influences of temperature, sample loadings, adsorption time, initial metal ion concentrations, and pH on the efficiency of the metal ions adsorption process were investigated. The thermodynamics and kinetics of Cu (II) adsorption for both the raw seaweed and seaweed residue were studied in order to determine the maximum removal efficiency and capacity. The characterization of the seaweed and seaweed residue before and after copper adsorption with SEM, FTIR, EDS, etc., coupled with the thermodynamics study, confirmed the ion exchange mechanism involved in the adsorption process. Under optimal conditions, the removal efficiencies were 75% and 71% for *L. nigrescens* and seaweed residue, respectively, and the adsorption capacities can reach 12.15 mg/g and 9.09 mg/g within 10 min for *L. nigrescens* and seaweed residue, respectively. The slight reduction in removal efficiency was because the active ion exchange sites were partially removed during the alginate extraction. The comparable metal ion removal efficiency between raw seaweed and seaweed residue suggesting the *L. nigrescens* residue is viable as bio-adsorbent and potential for industrial applications in adsorption process. The results provided a novel way to upgrade seaweed biomass in a biorefinery concept.

**Keywords:** brown seaweed residue; heavy metal removal; bioadsorption



**Citation:** Chen, H.; Zhang, R.; Qu, X.; Yuan, Y.; Zhu, B.; Zhao, S.; Jiang, T. Adsorption Properties and Mechanism of Copper Ions from Wastewater by *Lessonia nigrescens* and *Lessonia nigrescens* Residue. *Separations* **2023**, *10*, 559. https://doi.org/10.3390/separations10110559

Academic Editor: Gavino Sanna

Received: 9 October 2023
Revised: 1 November 2023
Accepted: 1 November 2023
Published: 5 November 2023



## 1. Introduction

Nowadays, the unavoidable use of heavy metals has led to water and soil pollution, becoming an increasingly urgent environmental problem [1,2]. Due to their high toxicity and resistance to environmental metabolism, even at low concentrations, heavy metals can be accumulated by aquatic organisms in water, leading to biomagnification in the food chain and ultimately affecting the safety of underwater organisms as well as human beings [3,4]. For example, lead poisoning can damage the nervous system [5], and exposure to arsenic can lead to cognitive impairments and growth retardation [6,7]. Copper is not poisonous as a metal and is also an essential trace mineral, which is extremely important for human health. However, Cu is toxic when forming compounds, such as copper sulfate, copper carbonate, and copper sub-acetate [8]. Excessive exposure to Cu can also influence

human health and stimulate the digestive system, causing abdominal pain, vomiting, and potential liver damage. It is reported that long-term consumption of water with excessive copper content can lead to cirrhosis and cardiovascular diseases [9–12]. Many instances of copper toxicity are often associated with accidental consumption or installation of contaminated water sources; therefore, it is important to remove Cu from the environment. Various techniques, such as ion exchange [13], membrane filtration [14], chemical precipitation [15], and electrochemical methods [16] have been applied to remove $Cu^{2+}$ from contaminated water. However, these methods are normally associated with high costs, potential secondary pollution, and complex operations, making them difficult to apply in practical applications [17,18]. In comparison, the bioadsorbent and bioadsorption process, with its characteristics of simple operation, low cost, strong adsorption capacity, and absence of secondary pollution, is the preferred option for heavy metal removal [19–21].

*Lessonia nigrescens* is a type of brown seaweed that is mainly distributed along the Chilean coast in the South Pacific [22]. This seaweed can grow up to several meters in length, with the longest specimens reaching up to 200 to 300 m. Due to its large size, rapid growth rate, and high alginate content, *Lessonia nigrescens* is widely used for the production of alginates [23]. Alginate is an important sustainable and renewable natural gelling material that has been widely applied in various fields, such as food, medicine, and cosmetics. The global market for alginate has continuously risen in recent years and is estimated to be over USD700 million in 2025 [24]. Depending on the seaweed species, harvesting season and extraction parameters, the yield of alginate is normally between 17–40%. Unavoidably, significant amount of seaweed residue is generated every year which is discarded as waste [25]. However, these seaweed residues are of great value because some functional groups such as -OH, $-SO_3H$, and $-COO^-$ are remaining. These functional groups can potentially act as reducing agent or chelating agent for various applications including heavy metal adsorption. Therefore, using seaweed residue as heavy metal bioadsorbent is one of the important approaches to enhance the economic value of seaweed and research on the use of algal residue as heavy metal adsorbent is increasing [26].

The research conducted by Héctor A. Cid et al. on the adsorption of $Cu^{2+}$ by brown seaweed revealed that the seaweed captured $Cu^{2+}$ from solution via surface interactions involving different functional groups such as carboxyl, hydroxyl, sulfonic acid, and amide groups. These interactions occur via ion and coordination bonds, ligand polymorphism, and rearrangement of cell wall rigidity to adsorb metal ions [27]. Davis studied the extraction and purification of alginates from macroalgae and concluded that the main factors influencing heavy metal adsorption are the content and composition of alginates, with particular emphasis on the presence of glucuronic acid residues [28]. Carvalho discovered that seaweeds depleted of alginates still exhibit excellent metal adsorption capabilities. This suggests that although the extraction of alginates from brown algae can hinder metal ion adsorption, in some cases, alginates are not the main component responsible for the adsorption of heavy metal ions, and the alginate extraction procedure may destroy the algal cell wall, which will then expose other functional groups and therefore beneficial for heavy metal removal [29].

This study aims to explore the potential of $Cu^{2+}$ adsorption by utilizing *L. nigrescens* particles after extracting alginates. The adsorption ability of $Cu^{2+}$ by *L. nigrescens* particles and seaweed residue after extracting alginates from *L. nigrescens* was compared. Adsorption parameters such as pH value, initial concentration of $Cu^{2+}$, adsorbent dosage, adsorption time, and temperature were considered to investigate their impacts on the adsorption process. Additionally, elemental analysis, spectroscopic analysis, and adsorption isotherm and kinetic models were used to explore the mechanism of $Cu^{2+}$ adsorption by *L. nigrescens* particles and seaweed residue.

## 2. Materials and Methods

### *2.1. Raw Materials and Chemicals*

The brown seaweed, *Lessonia nigrescens*, was kindly supplied by Bright Moon Seaweed Group, Qingdao, China, and was washed with tap water before drying in the oven at 60 °C until constant weight. The dried seaweed was then ground into particles (1 mm × 1 mm) and stored in dry, sealed containers. 27 mg DDTC-Na ($C_5H_{10}NNaS_2 \cdot 3H_2O$, Rhawn) was dissolved in 500 mL water as a chromogenic agent. Copper stock solution (5000 mg $L^{-1}$) was prepared by dissolving 0.3911 g $CuSO_4 \cdot 5H_2O$ (Gaojing chemical plant) into 50 mL water, and then different concentrations of copper solutions (0–500 mg $L^{-1}$) were obtained by diluting copper stock solution as appropriate. $Na_2CO_3$ was purchased from Rhawn. Ammonia solution was purchased from Rhawn.

### *2.2. Residue Seaweed Preparation*

The *L. nigrescens* particles (2 g) were mixed with 150 mL $Na_2CO_3$ solution (15 g $L^{-1}$). The mixture was stirred at 200 rpm under magnetic stirring for 60 min at 60 °C, and then the mixture was filtered to separate the liquid and solids. Filtered *L. nigrescens* residue was washed with Milli Q water and dried in the oven at 60 °C until constant weight.

### *2.3. Characterization of Original Seaweed Particles and the Seaweed Particles after $Cu^{2+}$ Adsorption*

The size and morphology of the *L. nigrescens* particles were visualized by scanning electron microscopy (SEM, Zeiss Sigma VP HD). Molecular information was characterized by FTIR. FTIR spectra were recorded using Thermo Scientific Nicolet iS20 scanning (Thermofisher, Waltham, MA, USA) from 4000–400 $cm^{-1}$. All spectra were collected with 32 scans and analyzed using Opus 7.0 software. The presence and related content of metals on the seaweed surface were analyzed using Energy-Dispersive X-ray Spectroscopy (EDS).

### *2.4. $Cu^{2+}$ Removal by L. nigrescens Particles and Seaweed Residue*

*L. nigrescens* particles or seaweed residue (50 mg) were mixed with 5 mL of different concentrations of $Cu^{2+}$ solutions (12.5, 50, 100, 200, 400, 800 mg $L^{-1}$) for the effect of the initial $Cu^{2+}$ concentration investigation. The mixture was stirred at 200 rpm under magnetic stirring for 60 min and then filtered to separate the liquid and solids. 1 mL of the supernatant was mixed with 3 mL of the DDTA-Na solution for color development. After incubation at room temperature for 5 min, the absorbance of 452 nm was recorded using UV-Vis Spectrometer (Jinghua, 723, Shanghai Jinghua Technology Instrument Co., Ltd., Shanghai, China). Calibration curves were obtained using 1 mL of $Cu^{2+}$ solutions (12.5, 25, 50, 100, and 200 mg $L^{-1}$) under the above procedure. Adsorption of copper by *L. nigrescens* can be calculated by:

$$q_t = \frac{(C_0 - C_t)V}{W} \quad (1)$$

where $C_0$ is the initial concentration of the metal ion (mg $L^{-1}$); $C_t$ is the concentration of the metal ion in the liquid phase after adsorption (mg $L^{-1}$); V is the volume of the solution (L); and W is the mass of adsorbent applied (g). The resulting solid seaweed residue was washed with distilled water three times and dried at 60 °C until constant weight for further analysis.

The mixture of *L. nigrescens* particles (50 mg) and 5 mL of $Cu^{2+}$ solutions (200 mg $L^{-1}$) were stirred at 200 rpm for different contact times (1, 3, 5, 10, 15, 30 min) for the effect of contact time investigation. After stirring, the mixture was filtered to separate the liquid and solids. The subsequent analyses and calculations of metal ion concentrations of the supernatants were the same as described above.

The *L. nigrescens* particles (50 mg) were mixed with 5 mL of $Cu^{2+}$ solutions (200 mg $L^{-1}$) at different pH values (4, 5, 6, 7, 8) for the effect of pH investigation. The pH of the $Cu^{2+}$ solution was adjusted with a diluted ammonia solution. The mixture was under magnetic stirring for 10 min at 200 rpm and then filtered to separate the liquid and solids. The

subsequent analyses and calculations of metal ion concentrations of the supernatants were the same as described above.

The *L. nigrescens* particles (50 mg) were mixed with 5 mL $Cu^{2+}$ solution (200 mg $L^{-1}$). The mixture was under magnetic stirring for 10 min at different temperatures (30, 40, 50, 60 °C) and then filtered to separate the liquid and solids for the effect of temperature investigation. The subsequent analyses and calculations of metal ion concentrations of the supernatants were the same as described above.

Different qualities of the *L. nigrescens* particles (12.5, 25, 50, 100, 200, 400 mg) were mixed with 5 mL $Cu^{2+}$ solution (200 mg $L^{-1}$) for the effect of *L. nigrescens* quality investigation. The mixture was under magnetic stirring for 10 min at 200 rpm and then filtered to separate the liquid and solids. The subsequent analyses and calculations of metal ion concentrations of the supernatants were the same as described above.

### *2.5. Adsorption Isotherms*

Experimental data of $Cu^{2+}$ adsorption by *L. nigrescens* particles and seaweed residue were fitted to Langmuir and Freundlich models to describe the adsorption isotherms. The Langmuir equation can be expressed as:

$$\frac{C_e}{q_e} = \frac{1}{q_{max} K_L} + \frac{C_e}{q_{max}} \quad (2)$$

where $q_e$ is the equilibrium removal capacity (mg/g), $q_{max}$ is the amount of heavy metal adsorbed in a complete monolayer (mg/g), $C_e$ is the equilibrium concentration of metal ions (mg/L), and $k_L$ is the Langmuir constant (L/mg). $q_{max}$ and $K_L$ can be determined from a linear plot according to Equation (3).

The Freundlich Equation can be expressed as:

$$\ln q_e = \ln K_F + \frac{1}{n} \ln C_e \quad (3)$$

where $q_e$ is the equilibrium removal capacity (mg/g), $C_e$ is the equilibrium metal ion concentration in the supernatant (mg/L), $K_F$ is the Freundlich constant, and 1/n is the adsorption intensity. $K_F$ and 1/n can be determined from a linear plot according to Equation (3).

### *2.6. Adsorption Kinetics*

The pseudo-second-order kinetic parameters using rate-controlling steps of chemical adsorption can be described by Equation (4).

$$\frac{t}{q_t} = \frac{1}{K_2 q_e^2} + \frac{t}{q_e} \quad (4)$$

where $q_t$ is the adsorption capacity at time t (mg/g), $k_2$ is the pseudo-second-order rate constant pseudo-second-order kinetic model (g/mg min), and $q_e$ is the adsorption capacity at equilibrium (mg/g).

The pseudo-first-order kinetic model considers that the occupancy rate of adsorption sites is directly proportional to the number of unoccupied sites. It can be written as:

$$\left(\frac{dq_t}{dt}\right) = k_1(q_e - q_t) \quad (5)$$

where $q_t$ is the adsorption capacity at time t (mg/g), $q_e$ is the adsorption capacity at equilibrium (mg/g), and $k_1$ is the pseudo-first-order rate constant (g/mg min).

The Elovich model describes the kinetic process of gas-chemical adsorption on the surface of adsorbents. The specific form of the Elovich diffusion model is described as follows:

$$q_t = \frac{1}{\beta} \ln(\alpha\beta) + \frac{1}{\beta} \ln t \quad (6)$$

where $q_t$ is adsorption capacity at time t (mg/g). $\alpha$ and $\beta$ are the initial adsorption rate and desorption constant, respectively.

The intraparticle diffusion model was established by Weber and Morris to explore the internal diffusion mechanism and diffusion process. The specific form of the intraparticle diffusion model is described as follows:

$$q_t = k_{di} t^{\frac{1}{2}} + C \quad (7)$$

where C is the constant of the boundary layer (mg/g). $k_{di}$ is the intraparticle diffusion rate (mg/g $min^{0.5}$). $q_t$ is the adsorption capacity at time t (mg/g).

### *2.7. Adsorption Thermodynamics*

The thermodynamic behavior of the adsorption of $Cu^{2+}$ on *L. nigrescens* was evaluated, and the thermodynamic parameters, including the Gibbs free energy change ($\Delta G^0$), enthalpy change ($\Delta H^0$), and entropy change ($\Delta S^0$), were determined according to the following Equations (8) and (9):

$$K = q_e / C_e \quad (8)$$

$$\Delta G^0 = -RTlnK \quad (9)$$

$$lnK = \frac{\Delta S^0}{R} - \frac{\Delta H^0}{RT} \quad (10)$$

where R is the universal gas constant, 8.314 $J \cdot mol^{-1} \cdot K^{-1}$; T is the Kelvin temperature (K); $q_e$ is the adsorption capacity of the adsorbent at the equilibrium (mg $g^{-1}$); $C_e$ is the residual $Cu^{2+}$ concentration at equilibrium (mg $L^{-1}$).

## 3. Result and Discussion

### *3.1. Characterization of the Seaweed Particles*

The SEM images of the *Lessonia Nigrescens* particles, the *L. nigrescens* particles after $Cu^{2+}$ adsorption, the seaweed residue, and the seaweed residue after $Cu^{2+}$ adsorption are shown in Figure 1a–d. According to Figure 1a, the intact cell structure can be observed from the *L. nigrescens* particles, and the cell diameter of *L. nigrescens* is approximately 20–30 μm. For the seaweed residue (Figure 1c), the cellular structure is more crowded and wrinkled, with a significant reduction in cell diameter. This is because alginates are important constituents of seaweed cell walls, providing them with structural strength and stability. When alginates are extracted and the cells lose their support, the cell walls are collapsed and fold, resulting in wrinkling. However, after one cycle of $Cu^{2+}$ adsorption, significant damage to the cell structure of both *L. nigrescens* particles and seaweed residue was observed, with almost no observable cell structure remaining (Figure 1b,d).

FTIR spectroscopy has been frequently used to study the adsorption mechanisms between heavy metals and brown seaweed with respect to metal-carboxylate coordination [30], metal-phenolics coordination [31], metal-amino group coordination [32], etc., by detecting the vibrational frequency changes of carbonyl groups (-CO), hydroxyl groups (-OH) and amino groups ($-NH_2$). The FTIR spectra of the *L. nigrescens* particles, the *L. nigrescens* particles after $Cu^{2+}$ adsorption, the seaweed residue and the seaweed residue after $Cu^{2+}$ adsorption are shown in Figure 2a. The peaks at 3431 $cm^{-1}$ and 2924 $cm^{-1}$ were associated with O-H stretching vibration and C-H antisymmetric stretching vibration [33,34]. The peak at 1033 $cm^{-1}$ was due to the C-O-C stretching vibration from the carbohydrates in algal cell wall. The peaks centered around 1624 $cm^{-1}$ and 1417 $cm^{-1}$ were due to the asymmetric $COO^-$ and symmetric $COO^-$ stretching vibrations [35,36], mainly attributed by the naturally occurring alginates in the algal cell wall. Alginates are believed to be one of the most important biomaterials that involved in heavy metal adsorption in brown seaweed via ion exchange or formation of metal-alginate complex. From Figure 2b,

some changes of the spectra that related to the $COO^-$ stretching vibration can be observed before and after $Cu^{2+}$ adsorption for both *L. nigrescens* particles. Specifically, the peak at 1417 $cm^{-1}$ shifts to 1416 $cm^{-1}$ for *L. nigrescens* particles, and the peak at 1624 $cm^{-1}$ changes to 1623 $cm^{-1}$ for both *L. nigrescens* particles and seaweed residue. This may be attributed to the association of metal chelates formed by the adsorption of $Cu^{2+}$ by *Lessonia Nigrescens* particles and seaweed residue in a "pseudo bridged" unidentate arrangement, where one carboxylate group interacts with the metal ion while another forms a hydrogen bond with adjacent hydroxyl groups. The formation of hydrogen bonds can lead to an elongation of the C=O bond length, and the vibrational frequency of chemical bonds is inversely proportional to the square root of the bond length [37,38]. The peak at 819 $cm^{-1}$ is because of the presence of mannuronic acid [39–41]. By comparing the peaks around 817 $cm^{-1}$ in seaweed residue and *L. nigrescens* particles, it was found that the peak intensity in the seaweed residue was reduced (Figure 2a). This was attributed to the partially extraction of alginate, resulting in a small amount of residual alginate within the residue.

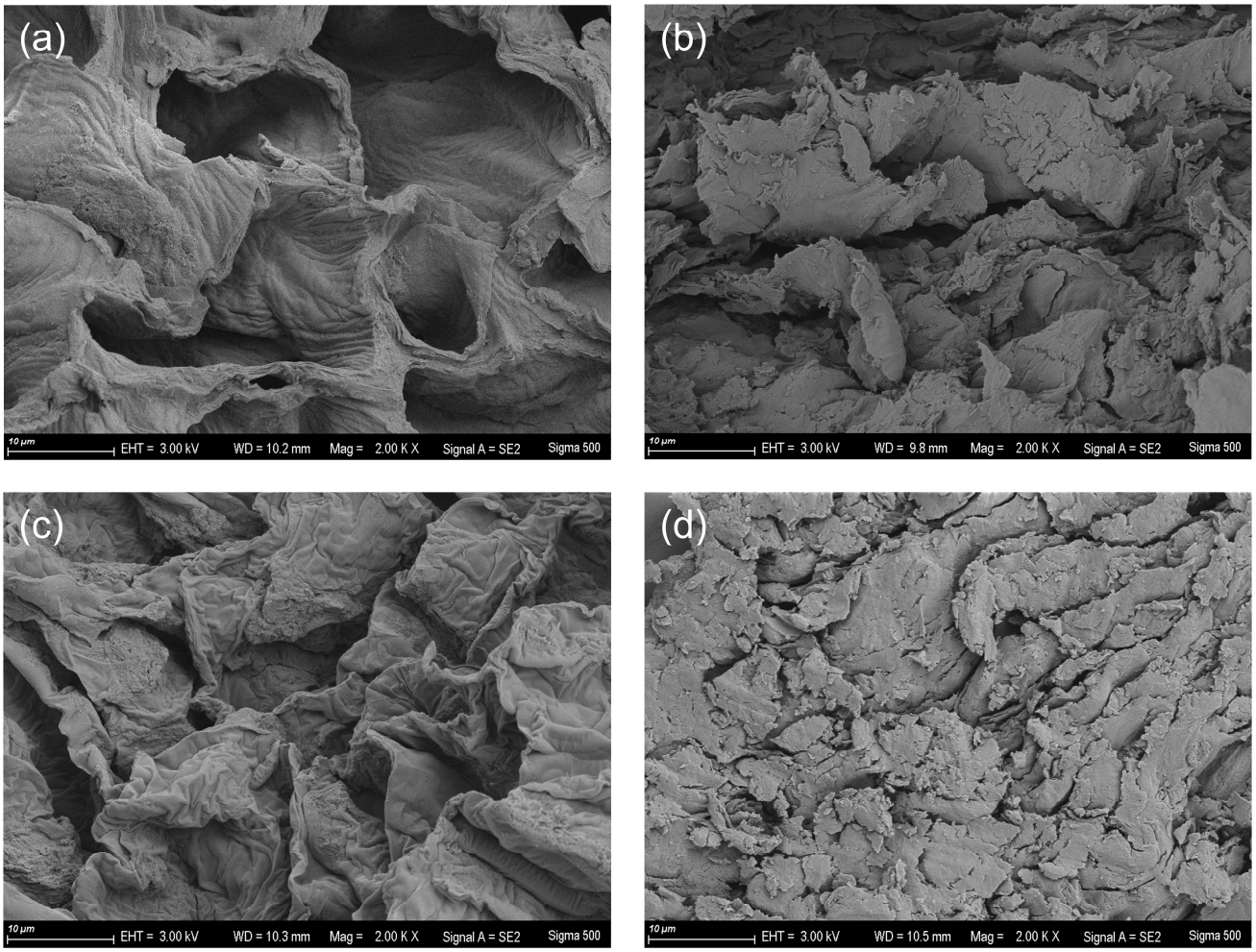


**Figure 1.** SEM images of the *L. nigrescens* particles (**a**), the *L. nigrescens* particles after $Cu^{2+}$ adsorption (**b**), the seaweed residue (**c**), and the seaweed residue after $Cu^{2+}$ adsorption (**d**).

Important cell wall components such as alginates and sulfated fucans in brown seaweed are ion exchangers for heavy metal adsorption, in which cations such as $Na^+$, $Mg^{2+}$, $K^+$, and $Zn^{2+}$ are substituted by heavy metal ions. Thus, in this study, EDS was used to characterize the elemental compositions and concentrations of *L. nigrescens* particles and seaweed residue surfaces before and after $Cu^{2+}$ adsorption for a better understanding of the adsorption mechanism. Figure 3 summarizes the changes in the content of elements of the *L. nigrescens* particles

and the seaweed residue before and after adsorption detected using EDS. From Figure 3, it can be observed that C and O were the main elements of both the *L. nigrescens* particles and seaweed residue, attributing to the carbohydrates in the algal cell wall. Na, K, Mg, and Ca were the primary metallic elements, and Cu was not detectable in either the *L. nigrescens* particles or the seaweed residue before adsorption. After adsorption, there were 1.28% and 0.39% $Cu^{2+}$ on the *L. nigrescens* particles and the seaweed residue surface, respectively. According to the batch adsorption experiments described in Section 3.2.3, removal percentage and removal capacity were 65.85%, 40.09%, and 26.34 mg/g, 16.04 mg/g, respectively. The disproportionality of the experimental data suggest a different adsorption mechanism of *L. nigrescens* particles and seaweed residue, where the adsorption of *L. nigrescens* particles was more likely to occur on the cell surface, while the seaweed residue was more likely to be co-adsorbed on the surface and inside the cell.

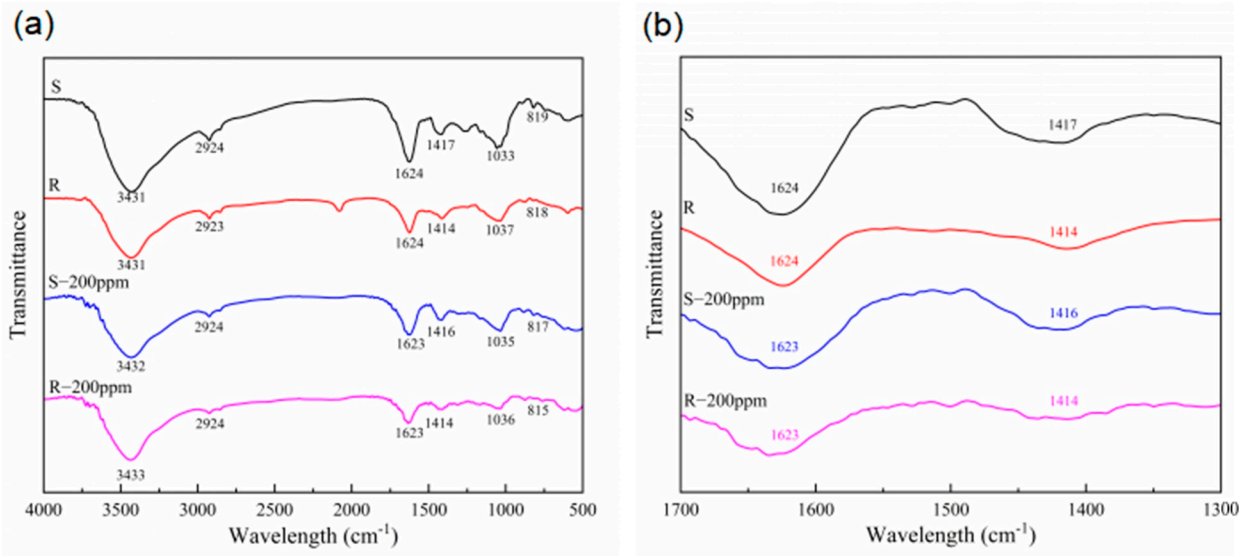


**Figure 2.** The FT − IR spectra of the *L. nigrescens* particles (S), the *L. nigrescens* particles after $Cu^{2+}$ adsorption (S − 200), the seaweed residue (R), and the seaweed residue after $Cu^{2+}$ adsorption (R − 200). Wavenumber from 4000 to 400 $cm^{-1}$ (**a**); wavenumber from 1700 to 1300 $cm^{-1}$ (**b**).

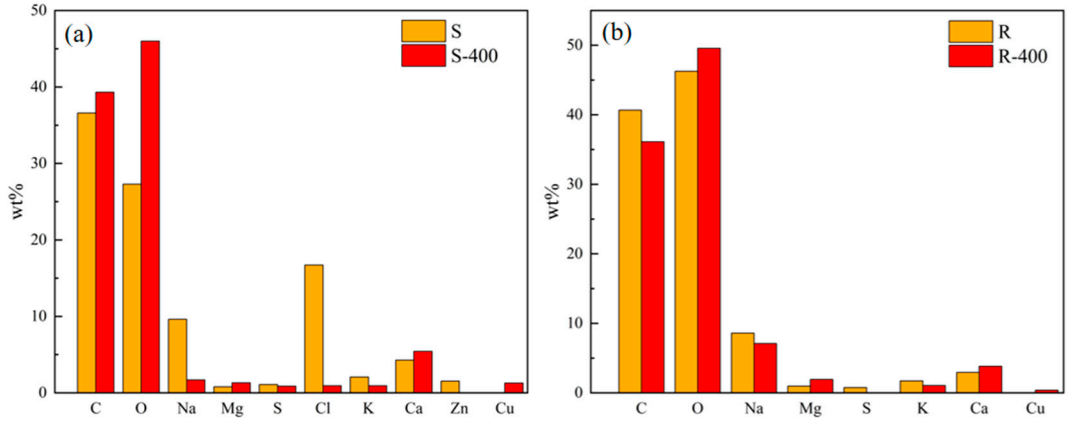


**Figure 3.** Comparison of elemental content in *L. nigrescens* particles before and after $Cu^{2+}$ adsorption (**a**), comparison of elemental content in seaweed residues before and after $Cu^{2+}$ adsorption (**b**).

Additionally, the surface of the *L. nigrescens* particles shows a significant amount of Na and Cl, which probably due to the sodium chloride was not fully removed when washing (Figure 3a). Additionally, the significant increase in carbon and oxygen content for *L. nigrescens* particles after adsorption was also due to the removal of sodium chloride, resulting in the proportional increase in other elements. A complete disappearance of Zn

was also observed for *L. nigrescens* particles after adsorption, suggesting Zn was totally replaced by Cu during adsorption. Compared to *L. nigrescens* particles, the seaweed residue lacks Zn on the cell surface due to the extraction of alginate. The reduction in Na and K in the seaweed residue after adsorption indicated that ion exchange occurred mainly among these elements (Figure 3b) [42].

### *3.2. $Cu^{2+}$ Adsorption by the L. nigrescens Particles and Seaweed Residues*

In order to further investigate the differences and mechanisms of $Cu^{2+}$ adsorption by the *L. nigrescens* particles and seaweed residues, as well as the potential of seaweed residue as adsorbents for heavy metals, batch adsorption experiments were conducted on the *L. nigrescens* particles and seaweed residue for $Cu^{2+}$ adsorption.

#### 3.2.1. Effect of Different Contact Time

The adsorption equilibrium time is an important parameter in the adsorption process. It plays an important role in understanding as well as controlling the dynamic behavior of adsorption, and most importantly, the fast adsorption process is beneficial for industrial scale-up. Figure 4 shows the variation of $Cu^{2+}$ uptake with time for *L. nigrescens* particles. The adsorption rate of *L. nigrescens* particles was extremely rapid within the first 10 min. When the initial concentration of $Cu^{2+}$ was 200 mg/L, approximately 12.15 mg of copper ions were adsorbed per 1 g of *L. nigrescens* particles in the initial 10 min, and the removal percentage reached 60.78%. After 10 min, the adsorption speed significantly slowed down, with only 12% increase in the removal efficiency for the next 50 min (Figure 4). The rapid metal uptake speed by seaweed agrees with other findings. For example, Jia et al. [43] studied chromium adsorption using different types of seaweeds, including kelp, sea lettuce, wakame, and laver. The removal efficiencies after 1 h were found to be 95.4%, 93.6%, 99.1%, and 57.2%, respectively, demonstrating the rapid heavy metal adsorption processes of seaweed.

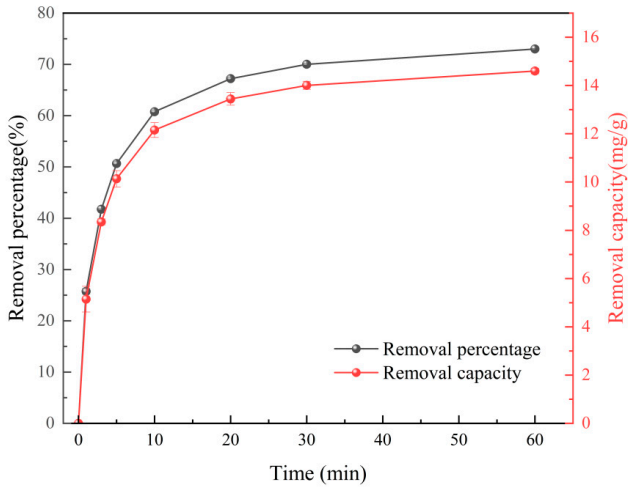


**Figure 4.** Effect of contact time on the adsorption of $Cu^{2+}$ onto *L. nigrescens* particles (black line: removal percentage, red line: removal capacity).

#### 3.2.2. Effect of Seaweed Loading

The effect of different amounts of *L. nigrescens* particles on adsorption efficiency and capacity of $Cu^{2+}$ adsorption was also investigated (Figure 5). With the increase of *L. nigrescens* particle mass from 0.0125 g to 0.4 g, the adsorption efficiency was improved from 43.6% to 81.2%. This was because as the amount of *L. nigrescens* particles increased, the number of active sites on the adsorbent also increased. However, a significant decrease in removal capacity was observed with the increasing amount of *L. nigrescens* particles, which was probably due to the fact that with the amount of seaweed increased, the mixture

was more difficult to be homogeneously dispersed with stirring so that longer stirring time may be required to reach adsorption equilibrium.

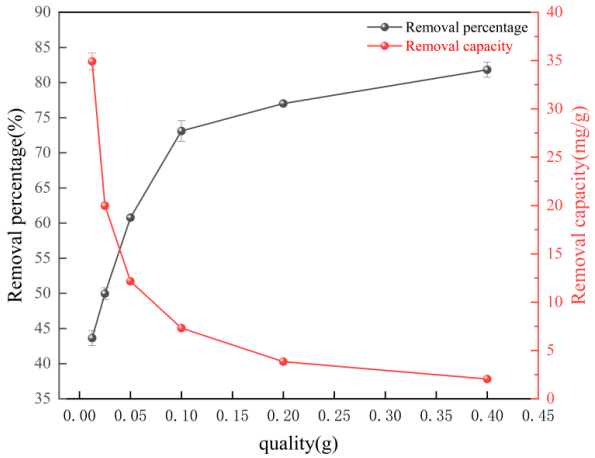


**Figure 5.** Seaweed quality on the adsorption of $Cu^{2+}$ onto *L. nigrescens* particles (black line: removal percentage, red line: removal capacity).

### 3.2.3. Effect of Initial $Cu^{2+}$ Concentration

To study the effect of initial $Cu^{2+}$ concentration on the amount of metal uptake by both the *L. nigrescens* particles and seaweed residue, the adsorption behaviors with $Cu^{2+}$ concentrations increasing from 100 mg/L to 800 mg/L were investigated (Figure 6). From Figure 6, we can conclude that *L. nigrescens* particles and seaweed residue showed similar adsorption patterns with the increasing of the initial $Cu^{2+}$ concentrations. According to the results, it can be observed that as the initial $Cu^{2+}$ concentration of the solution increased, the adsorption capacity continuously increased while the removal efficiency decreased. When the initial concentration of $Cu^{2+}$ increased from 100 mg/L to 800 mg/L, the adsorption capacity increased from 6.23 mg/g to 37.58 mg/g. This was because as the $Cu^{2+}$ concentration increases, the unoccupied adsorption sites start interacting with $Cu^{2+}$, leading to an increase in the adsorption capacity until the adsorbent approaches saturation.

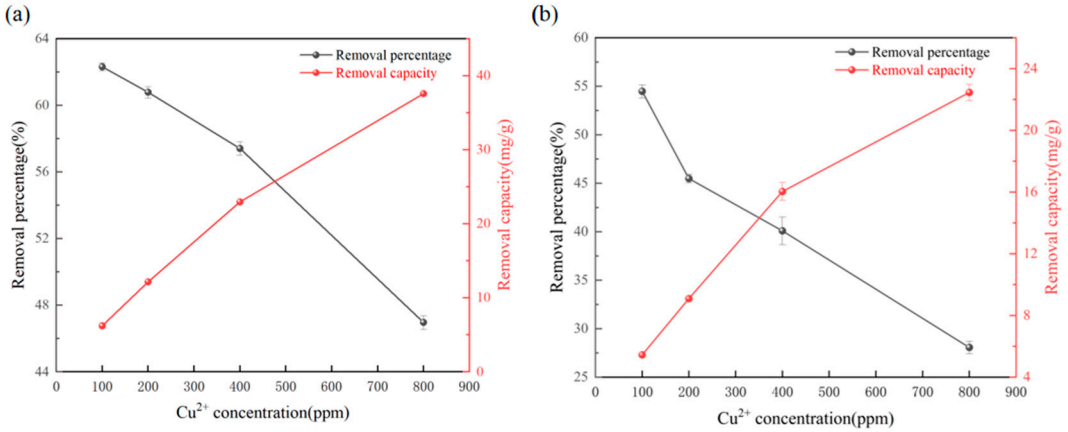


**Figure 6.** Effect of different initial $Cu^{2+}$ concentrations on $Cu^{2+}$ removal from aqueous solutions by the *L. nigrescens* particles (**a**), the effect of different initial $Cu^{2+}$ concentrations on $Cu^{2+}$ removal from aqueous solutions by the seaweed residue (**b**) (black line: removal percentage, red line: removal capacity).

Langmuir and Freundlich isotherm models are commonly used to describe the adsorption equilibrium and analyze the adsorption mechanisms [44–46]. The Langmuir adsorption isotherm model assumes that adsorption occurs on a monolayer surface or a homogenous surface with identical positions. The Freundlich adsorption isotherm model

assumes that adsorption occurs on a heterogeneous surface with multiple layers, and the adsorption capacity increases infinitely with an increase in $Cu^{2+}$ concentration [47]. The adsorption isotherms and the isotherm modeling data are shown in Figure 7 and Table 1. From Figure 7a,b, it can be observed that compared to the Freundlich model ($R^2$ = 0.9686), the adsorption of $Cu^{2+}$ by *L. nigrescens* particle is better described by the Langmuir model ($R^2$ = 0.9988), suggesting that *L. nigrescens* particles primarily underwent monolayer adsorption when the copper concentrations were ranging from 200 mg/L to 800 mg/L. From Figure 7c,d, it can be concluded that both the Langmuir model ($R^2$ = 0.9915) and the Freundlich model ($R^2$ = 0.9869) fit well for seaweed residue, suggesting a more complicated adsorption mechanism compared to *L. nigrescens* particles. The maximum Langmuir monolayer adsorption capacity of the *L. nigrescens* particles and seaweed residue, $q_{max}$ (mg/g), are 77.2 and 31.9, respectively (Table 1). The differences could be attributed to the lack of adsorption sites for seaweed residue due to the alginate extraction.

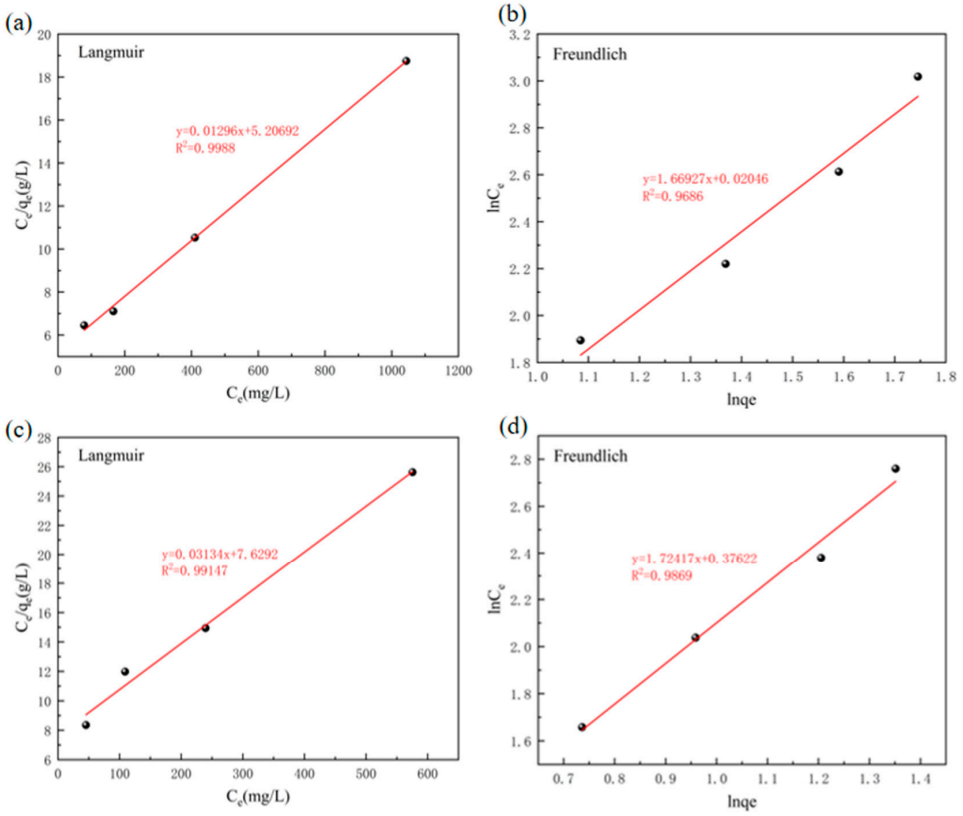


**Figure 7.** Langmuir (**a**) and Freundlich (**b**) isotherms for $Cu^{2+}$ adsorption on the *L. nigrescens* particles, Langmuir (**c**) and Freundlich (**d**) isotherms for $Cu^{2+}$ adsorption on the seaweed residues.

**Table 1.** Adsorption isotherm modeling data.

| Adsorbent | Model | Parameter | Value | $R^2$ |
|---|---|---|---|---|
| *L. nigrescens* particles | Langmuir | $K_L$ (L $mg^{-1}$) | 0.0025 | 0.9988 |
| | | $q_{max}$ (mg $g^{-1}$) | 77.165 | |
| | Freundlich | $K_F$ (mg $g^{-1}$) ($L\ mg^{-1})^{1/n}F$) | 0.9878 | 0.9686 |
| | | N (-) | 1.6693 | |
| Seaweed residue | Langmuir | $K_L$ (L $mg^{-1}$) | 0.0041 | 0.99147 |
| | | $q_{max}$ (mg $g^{-1}$) | 31.908 | |
| | Freundlich | $K_F$ (mg $g^{-1}$) ($L\ mg^{-1})^{1/n}F$) | 0.8039 | 0.9869 |
| | | N (-) | 1.7242 | |

3.2.4. Effect of Temperature

The influence of temperature on the adsorption capacity of metal ions is mainly manifested via its impact on the chemical structure of the adsorbent surface and the physicochemical properties of the solution [48]. As shown in Figure 8a, the adsorption efficiency of the *L. nigrescens* particles for $Cu^{2+}$ significantly increased with the increasing of temperature. At temperatures of 30 °C, 40 °C, 50 °C, and 60 °C, the adsorption efficiencies were 63.54%, 64.03%, 67.01%, and 67.54%, respectively. For seaweed residue, the adsorption efficiencies of 200 mg/L $Cu^{2+}$ at temperatures of 30 °C, 40 °C, 50 °C, and 60 °C were 50.78%, 53.97%, 58.24%, and 62.73%, respectively. The increasing of temperature is advantageous to the present adsorption processes since higher temperature activates the metal ions for enhancing the adsorption at the coordinating sites of the mineral.

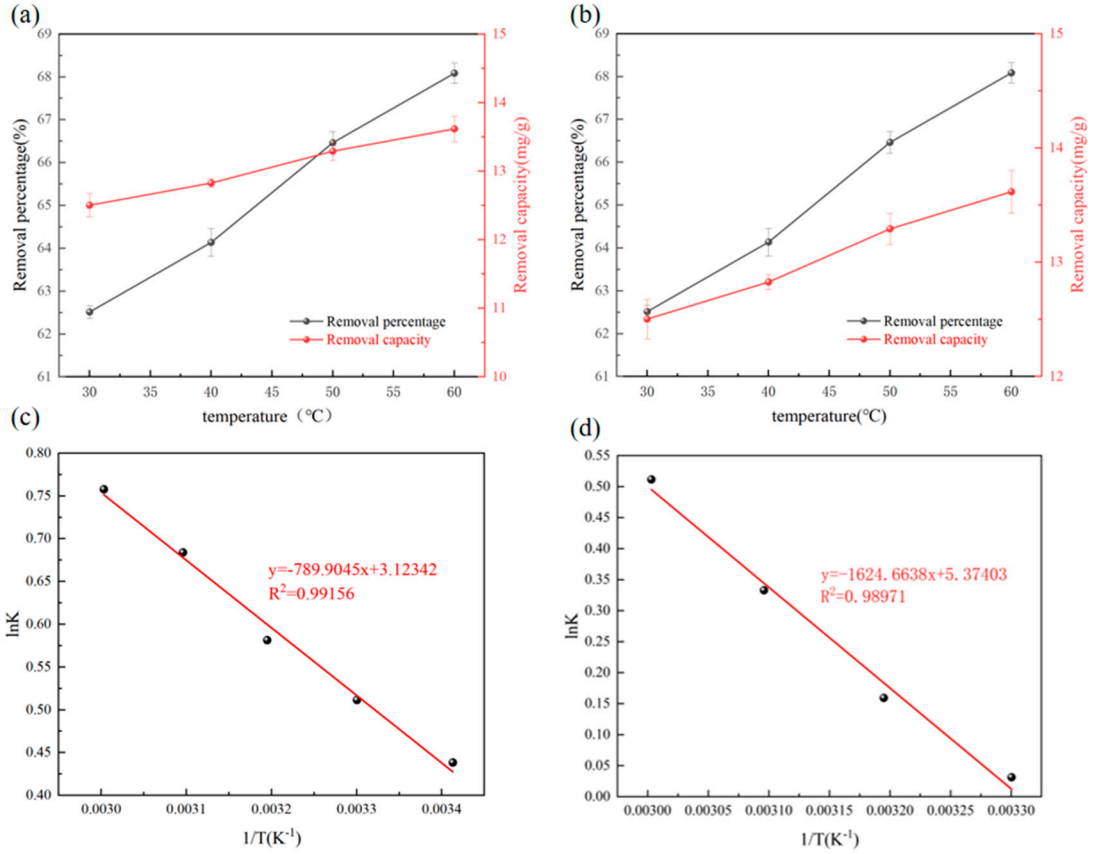


**Figure 8.** Effect of different temperatures on $Cu^{2+}$ removal from aqueous solutions by the *L. nigrescens* particle (**a**) and the seaweed residue (**b**) (black line: removal percentage, red line: removal capacity), Va not Hoff plot of the *L. nigrescens* particles (**c**) and seaweed residue (**d**).

The thermodynamic behavior of $Cu^{2+}$ adsorption on *L. nigrescens* particles and seaweed residue was determined by calculating the thermodynamic parameters, including the changing of Gibbs free energy ($\Delta G^0$), the enthalpy ($\Delta H^0$) and the entropy ($\Delta S^0$) according to Formulas (8)–(10) [49,50]. Table 1 summarizes the thermodynamic parameters obtained from the intercepts and slopes of the Va, not the Hoff plot (Figure 8c,d). A positive value of $\Delta H^0$ indicates that the adsorption of $Cu^{2+}$ by the *L. nigrescens* particles and seaweed residue is an endothermic process, which is consistent with the isotherm data showing an increase in adsorption capacity with temperature. The negative values of Gibbs free energy for $Cu^{2+}$ adsorption by seaweed and seaweed residue in the studied temperature range demonstrate the adsorption processes occurred spontaneously. When comparing the $\Delta G$ values of the same temperature between seaweed and seaweed residue adsorption processes, *L. nigrescens* particles always showed more negative values (Table 2), indicating it is more thermodynamically

favorable for *L. nigrescens* particles than seaweed residue. Adsorption entropy ($\Delta S^0$) represents the degree of disorder at the interface between the adsorbent and the adsorbate during the adsorption process. A value of $\Delta S^0$ for seaweed residue was larger than *L. nigrescens* particles, which means that the degree of randomness in the solid/solution interface of *L. nigrescens* particles was larger than that of seaweed residue.

**Table 2.** Calculated Thermodynamic Parameters.

| | ***L. nigrescens* Particles** | | | **Seaweed Residue** | | |
|---|---|---|---|---|---|---|
| **T (K)** | **$\Delta G^0$ (kJ·mol$^{-1}$)** | **$\Delta H^0$ (kJ·mol$^{-1}$)** | **$\Delta S^0$ (J·mol$^{-1}$·K$^{-1}$)** | **$\Delta G^0$ (kJ·mol$^{-1}$)** | **$\Delta H^0$ (kJ·mol$^{-1}$)** | **$\Delta S^0$ (J·mol$^{-1}$·K$^{-1}$)** |
| 303 | −1.2886 | 6.5673 | 25.9681 | −0.0787 | 13.5019 | 44.6797 |
| 313 | −1.5129 | | | −0.4143 | | |
| 323 | −1.8369 | | | −0.8937 | | |
| 333 | −2.0978 | | | −1.4161 | | |

### 3.2.5. Effect of pH

The pH value of the initial solution is an important factor that influences the bioadsorption process, which affects the type and number of functional groups on the seaweed or seaweed residue surfaces [51,52]. Thus, the adsorption experiments were conducted by adjusting the pH within the range of 4–8 while keeping other parameters constant.

For the *L. nigrescens* particles (Figure 9a), When the pH was between 4–6, the adsorption efficiency increased with the increase in the initial pH. However, when the pH was between 6–8, the adsorption efficiency rapidly decreased with the increase in pH. At low pH, the functional groups on the cell surface undergo protonation, which reduces the adsorption possibility of heavy metal cations from the solution [53]. Additionally, the high concentration of free hydrogen ions in the solution competes with the heavy metal ions for the adsorption sites on the seaweed and seaweed residue surfaces [54]. Under weak acidic conditions, the concentration of $H^+$ in the solution is decreased, and the material surface exposes more active adsorption sites that can be occupied by $Cu^{2+}$ [55]. When the solution becomes alkaline, the carboxyl group undergoes an acid-base neutralization reaction, resulting in the formation of corresponding salts and water. The decrease in carboxyl groups leads to a reduction in adsorption sites; hence, the adsorption capacity of *L. nigrescens* particles was decreased when the pH values were 7 and 8. By comparison of seaweed residue and *L. nigrescens* particles, smaller changes of adsorption capacity were observed at high pH values (from 6 to 8) (Figure 9b), indicating different adsorption mechanisms of seaweed residue and the carboxyl groups were not the major functional groups that were chelating $Cu^{2+}$ for adsorption.

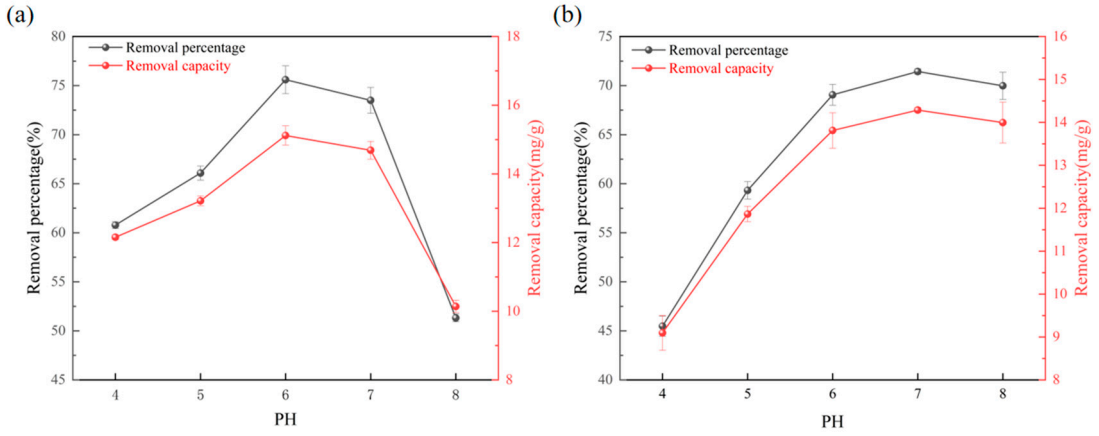


**Figure 9.** Effect of pH on $Cu^{2+}$ removal from aqueous solutions by the *L. nigrescens* particle (**a**), effect of pH on $Cu^{2+}$ removal from aqueous solutions by the seaweed residue (**b**) (black line: removal percentage, red line: removal capacity).

FT-IR was used to investigate the changes of carboxyl groups of seaweed and seaweed residue after $Cu^{2+}$ adsorption at different pH. From Figure 10a,b, it can be observed that carboxyl groups form coordination complexes with metal ions and undergo hydrogen bonding, resulting in changes in bond length and bond angles, which in turn cause shifts in wave numbers. Within the range of pH studied, the peak shape and peak position are almost the same. Similarly, Fuks et al. studied the Mn-alginate complex by FT-IR and found that pH did not influence the peak position and shape [56].

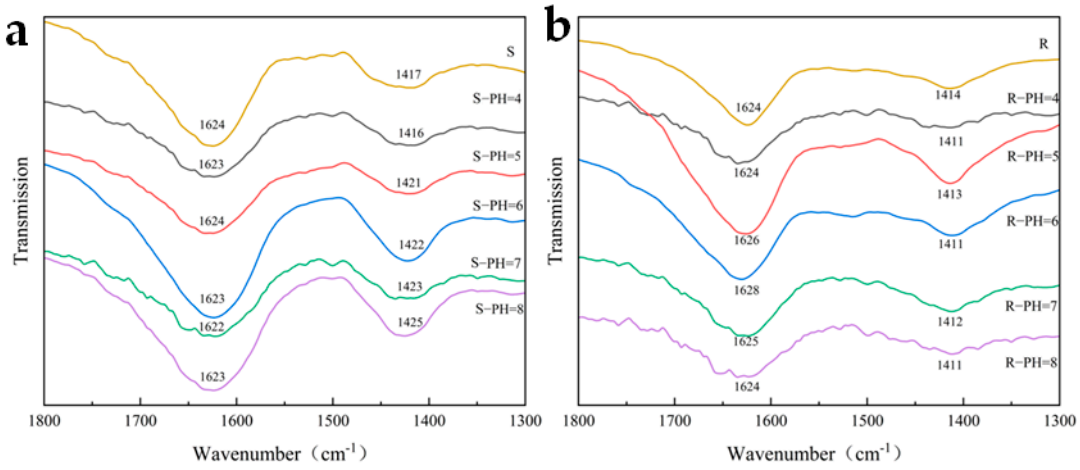


**Figure 10.** FT-IR spectra of the *L. nigrescens particles* (**a**) and seaweed residues (**b**) and the corresponding solids after $Cu^{2+}$ adsorption under different pH.

### 3.2.6. Regeneration of the Adsorbents and $Cu^{2+}$ Re-Adsorption

Figure 11 shows the adsorption efficiency of both *L. nigrescens* particles and seaweed residue during three adsorption cycles. From the results, we can conclude that a significant reduction in removal percentage was observed for *L. nigrescens* particles from the first adsorption cycle to the second adsorption cycle, and a slight reduction in removal percentage was observed from the second adsorption cycle to the third adsorption cycle. After three cycles, the adsorption efficiency was reduced from 60.8% to 40.8% for *L. nigrescens* particles. On the other hand, the removal efficiency was reduced from 45.5% to 38.8% after three adsorption cycles for seaweed residue. The reason for observing a greater adsorption efficiency decrease in *L. nigrescens* particles than seaweed residue for the second and third cycles may be because some of the adsorption sites of *L. nigrescens* particles were destroyed during the first adsorption cycle. Thus, the seaweed residue has the potential to be used in industrial wastewater remediation.

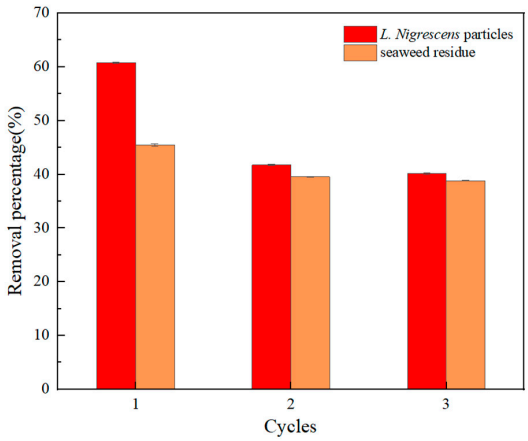


**Figure 11.** Re-adsorption of $Cu^{2+}$ by *L. nigrescens* particles and seaweed residue.

### 3.3. Kinetic Modeling

Adsorption kinetic data are important to predict the optimum operating conditions in experimental adsorption processes and help to design the adsorption system. Information such as adsorption mechanisms and potential rate-controlling steps can be provided by kinetic study [57]. Hence, in this study, kinetic models, including the Pseudo-first model, Pseudo-second order model, Elovich model, and Intraparticle diffusion model, were conducted by fitting the time adsorption curve. The kinetic fitting plots and parameters are concluded in Figures 12 and 13 and Table 3. The $R^2$ for the Pseudo-first model, Pseudo-second model, Elovich model, and Intraparticle diffusion model are 0.981, 0.997, 0.988, and 0.991, respectively.

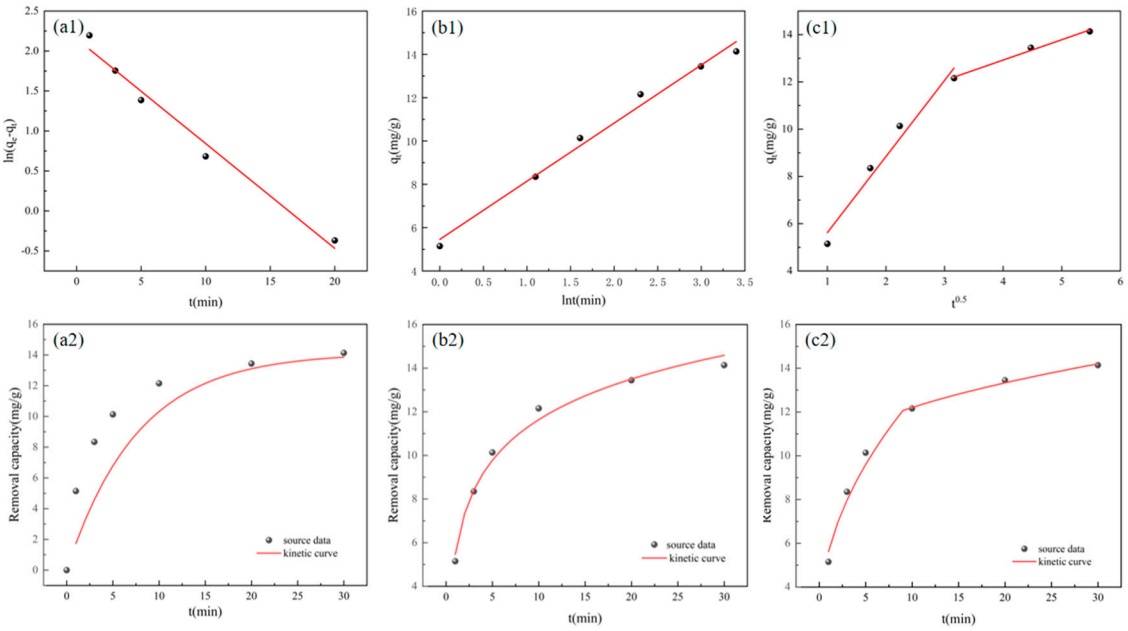


**Figure 12.** Pseudo-first-order kinetic model validation plot (**a1**) and kinetics comparison plot (**a2**); Elovich kinetic model validation plot (**b1**) and kinetics comparison plot (**b2**); Intraparticle diffusion model validation plot (**c1**) and kinetics comparison plot (**c2**).

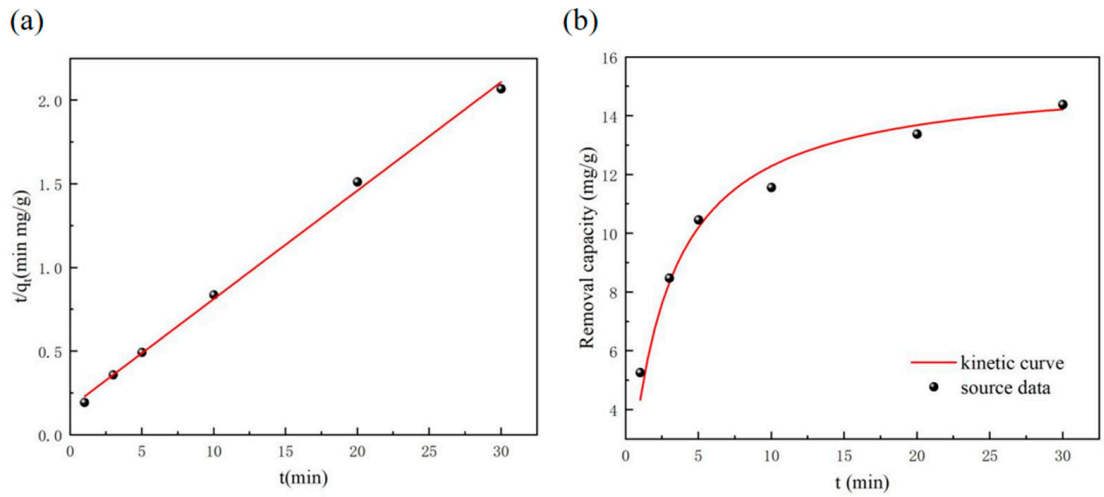


**Figure 13.** Pseudo-second-order kinetic model validation plot (**a**) and kinetics comparison plot (**b**) for $Cu^{2+}$ adsorption.

**Table 3.** Kinetic model parameters for Cu biosorption on *L. nigrescens* particles.

| **Model** | | **Model** | |
|---|---|---|---|
| Pseudo-first-order | | Elovich | |
| $k_1$ ($min^{-1}$) | 0.131 | α (mg/g min) | 20.5102 |
| $R^2$ | 0.981 | β (g/mg) | 0.3725 |
| | | $R^2$ | 0.988 |
| Pseudo-second-order | | Intraparticle diffusion | |
| $q_e$ (mg/g) | 15.129 | $k_{d1}$ (mg/g $min^{0.5}$) | 3.221 |
| $k_2$ (g/mg min) | 0.028 | $R^2$ | 0.984 |
| $R^2$ | 0.997 | $k_{d2}$ (mg/g $min^{0.5}$) | 0.861 |
| | | $R^2$ | 0.991 |

Important information such as adsorption rate and desorption rate can be obtained from the Elovich model by determining the initial adsorption rate α (mg/g min) and the desorption constant β (g/mg) [58]. According to Figure 12 and Table 3, the initial adsorption rate α was 20.5102 mg/g min, and the desorption constant β was 0.3725 g/mg in this study. Figure 12b shows the experimental data had good agreement with the theoretical data from the Elovich model.

Figure 12c represents the plot of $q_t$ versus $t^{0.5,}$ and two linear stages for $Cu^{2+}$ adsorption could be clearly observed by the intraparticle kinetic model. The kinetic parameters shown in Table 3 confirm such a two-stage linear relationship. The first stage was the rapid one ($K_{d1}$ = 3.221), whereas the second stage was much slower ($K_{d2}$ = 0.861), which was probably because the first stage represents the diffusion of $Cu^{2+}$ to the algal surface, whereas the second stage represents intraparticle diffusion. However, neither of these two linear stages passes through the origin, indicating that although the intraparticle diffusion was involved in the adsorption process, it was not the only rate-limiting mechanism.

In the case of the pseudo-second-order kinetic model, the adsorption efficiency is assumed to be directly proportional to the number of available sites, and it is independent of the initial concentration of the adsorbate [59]. The adsorption data of $Cu^{2+}$ onto the *L. nigrescens* particles was fitted using the Pseudo-second order model (Equation (4)). The linear plot of $t/q_t$ against t can give the pseudo-second-order adsorption rate constant k from the slope and qe from the intercept (Figure 13a). The correlation coefficient ($R^2$) was found to be 0.997, indicating that the adsorption kinetics of $Cu^{2+}$ onto the *L. nigrescens* particle can be well-fitted using the Pseudo-second order model (Figure 13). Thus, the efficiency-limiting step of the $Cu^{2+}$ adsorption onto *L. nigrescens* particles process may be dominated by chemical adsorption processes, where the formation of metal-organic compounds and ion exchange are the rate-controlling steps [60].

## 4. Conclusions

This article investigates the adsorption processes and influencing factors by controlling the adsorption conditions, including time, temperature, pH, and amount of biomass of $Cu^{2+}$ removal from wastewater by brown seaweed *L. nigrescens* particles and seaweed residue. It was found that the seaweed residue, after extraction of alginates, and the *L. nigrescens* particles exhibited effective removal of copper from aqueous solutions. The *L. nigrescens* particles and seaweed residue can achieve adsorption capacities of 12.15 mg/g and 9.09 mg/g, respectively, within 10 min. The study successfully validated that the adsorption of *L. nigrescens* particles and seaweed residue follows the mechanism of monolayer adsorption and chemical adsorption process by fitting the experimental data to a pseudo-second-order kinetic model and Langmuir isotherm. Although slightly lower removal efficiency and removal capacity have been observed for seaweed residue, there is still a potential for it to be used as a bioadsorbent because of its considerable $Cu^{2+}$ adsorption capacity. Overall, brown seaweed residue is worth further investigation as an environmentally friendly heavy metal adsorbent on a large scale.

**Author Contributions:** Conceptualization, R.Z. and T.J.; Methodology, H.C., R.Z. and S.Z.; Fromal analysis, H.C. and X.Q.; Investigation, H.C. and X.Q.; Data curation: H.C. and X.Q.; Resources, Y.Y. and B.Z.; Supervision, R.Z.; Writing-original draft, H.C.; Writing—review & editing: R.Z., Y.Y., B.Z., S.Z. and T.J. All authors have read and agreed to the published version of the manuscript.

**Funding:** This research was funded by Open Foundation of the Key Laboratory of Seaweed Fertilizers, Ministry of Agriculture of Rural Affairs (KLSF-2023-007).

**Data Availability Statement:** The data presented in this study are available on request from the corresponding author.

**Acknowledgments:** We thank the Open Foundation of the Key Laboratory of Seaweed Fertilizers, Ministry of Agriculture of Rural Affairs (KLSF-2023-007) for their financial support.

**Conflicts of Interest:** The authors declare no conflict of interest.

## References

1. Azimi, A.; Azari, A.; Rezakazemi, M.; Ansarpour, M. Removal of heavy metals from industrial wastewaters: A Review. *ChemBioEng Rev.* **2017**, *4*, 37–59. [CrossRef]
2. Nadeem, R.; Zafar, M.N.; Afzal, A.; Hanif, M.A.; Saeed, R. Potential of NaOH pretreated Mangifera indica waste biomass for the mitigation of Ni (II) and Co (II) from aqueous solutions. *J. Taiwan Inst. Chem. Eng.* **2014**, *45*, 967–972. [CrossRef]
3. Zhuang, Q.F.; Li, G.; Liu, Z.Y. Distribution, source and pollution level of heavy metals in river sediments from South China. *Catena Interdiscip. J. Soil Sci. Hydrol. Geomorphol. Focus. Geoecology Landsc. Evol.* **2018**, *170*, 386–389. [CrossRef]
4. Wei, C.Y.; Wang, C.; Yang, L.S. Characterizing spatial distribution and sources of heavy metals in the soils from mining-smelting activities in Shuikoushan, Hunan Province, China. *J. Environ. Sci.* **2009**, *21*, 1230–1236. [CrossRef] [PubMed]
5. Karri, V.; Schuhmacher, M.; Kumar, V. Heavy metals (Pb, Cd, As and MeHg) as risk factors for cognitive dysfunction: A general review of metal mixture mechanism in brain. *Environ. Toxicol. Pharmacol.* **2016**, *48*, 203–213. [CrossRef] [PubMed]
6. Zhang, Y.; Shang, P.; Wang, J.; Norris, P.; Romero, C.E.; Pan, W.P. Trace element (Hg, As, Cr, Cd, Pb) distribution and speciation in coal-fired power plants. *Fuel* **2017**, *208*, 647–654. [CrossRef]
7. Johri, N.; Jacquillet, G.; Unwin, R. Heavy metal poisoning: The effects of cadmium on the kidney. *Biometals* **2010**, *23*, 783–792. [CrossRef]
8. Zhang, W.; Pu, Q.; Mei, J.; Lin, F.; Zeng, Y.; Wang, W.; Li, W.; Liu, C.; Zhu, Y. Combined minimally invasive treatment of delayed aortoesophageal fistula caused by fishbone. *Ann. Thorac. Surg.* **2022**, *114*, e415–e418. [CrossRef]
9. Sun, J.H.; Chen, Y.; Yu, H.; Yan, L.; Du, B.; Pei, Z. Removal of $Cu^{2+}$, $Cd^{2+}$ and $Pb^{2+}$ from aqueous solutions by magnetic alginate microsphere based on $Fe_3O_4$/MgAl-layered double hydroxide. *J. Colloid Interface Sci.* **2018**, *532*, 474–484. [CrossRef] [PubMed]
10. De Rossi, A.; Rigueto, C.V.T.; Dettmer, A.; Colla, L.M.; Piccin, J.S. Synthesis, characterization, and application of Saccharomyces cerevisiae/alginate composites beads for adsorption of heavy metals. *J. Environ. Chem. Eng.* **2020**, *8*, 104009. [CrossRef]
11. Deze, E.G.; Papageorgiou, S.K.; Favvas, E.P.; Katsaros, F.K. Porous alginate aerogel beads for effective and rapid heavy metal sorption from aqueous solutions: Effect of porosity in $Cu^{2+}$ and $Cd^{2+}$ ion sorption. *Chem. Eng. J.* **2012**, *209*, 537–546. [CrossRef]
12. Jiang, H.; Yang, Y.; Lin, Z.; Zhao, B.; Zhang, A. Preparation of a novel bio-adsorbent of sodium alginate grafted polyacrylamide/graphene oxide hydrogel for the adsorption of heavy metal ion. *Sci. Total Environ.* **2020**, *744*, 140653. [CrossRef]
13. Alyuez, B.; Veli, S. Kinetics and equilibrium studies for the removal of nickel and zinc from aqueous solutions by ion exchange resins. *J. Hazard. Mater.* **2009**, *167*, 482–488. [CrossRef] [PubMed]
14. Haris, M.; Shakeel, A.; Hussain, T.; Ahmad, G.; Ansari, M.S.; Khan, A.A. New Trends in Removing Heavy Metals from Industrial Wastewater through Microbes. *Remov. Emerg. Contam. Through Microb. Process.* **2021**, 183–205. [CrossRef]
15. Chen, Q.; Yao, Y.; Li, X.; Lu, J.; Zhou, J.; Huang, Z. Comparison of heavy metal removals from aqueous solutions by chemical precipitation and characteristics of precipitates. *J. Water Process. Eng.* **2018**, *26*, 289–300. [CrossRef]
16. Chaplin, B.P. The Prospect of Electrochemical Technologies Advancing Worldwide Water Treatment. *Acc. Chem. Res.* **2019**, *52*, 596–604. [CrossRef] [PubMed]
17. Zhu, Y.; Fan, W.; Zhou, T.; Li, X. Removal of chelated heavy metals from aqueous solution: A review of current methods and mechanisms. *Sci. Total Environ.* **2019**, *678*, 253–266. [CrossRef]
18. Fu, F.; Wang, Q. Removal of heavy metal ions from wastewaters: A review. *J. Environ. Manag.* **2011**, *92*, 407–418. [CrossRef] [PubMed]
19. Burakov, A.E.; Galunin, E.V.; Burakova, I.V.; Kucherova, A.E.; Agarwal, S.; Tkachev, A.G.; Gupta, V.K. Adsorption of heavy metals on conventional and nanostructured materials for wastewater treatment purposes: A review. *Ecotoxicol. Environ. Saf.* **2018**, *148*, 702–712. [CrossRef]
20. Zafar, M.N.; Parveen, A.; Nadeem, R. A pretreated green biosorbent based on Neem leaves biomass for the removal of lead from wastewater. *Desalination Water Treat.* **2013**, *51*, 4459–4466. [CrossRef]
21. Fiyadh, S.S.; Alsaadi, M.A.; Jaafar, W.Z.; Alomar, M.K.; Fayaed, S.S.; Mohd, N.S.; Hin, L.S.; El-Shafie, A. Review on heavy metal adsorption processes by carbon nanotubes. *J. Clean. Prod.* **2019**, *230*, 783–793. [CrossRef]

22. Navarrete, I.A.; Kim, D.Y.; Wilcox, C.; Reed, D.C.; Wilcox, B.H. Effects of depth-cycling on nutrient uptake and biomass production in the giant kelp *Macrocystis pyrifera*. *Renew. Sustain. Energy Rev.* **2021**, *141*, 110747. [CrossRef]
23. Hansen, H.K.; Gutierrez, C.; Madrid, A.; Jimenez, R.; Larach, H. Possible use of the algae *Lessonia nigrescens* as a biosorbent: Differences in copper sorption behavior using either blades or stipes. *Waste Biomass Valorization* **2017**, *8*, 1295–1302. [CrossRef]
24. Kabir, I.I.; Sorrell, C.C.; Mofarah, S.S.; Yang, W.; Yuen, A.C.Y.; Nazir, M.T.; Yeoh, G.H. Alginate/polymer-based materials for fire retardancy: Synthesis, structure, properties, and applications. *Polym. Rev.* **2021**, *61*, 357–414. [CrossRef]
25. Cebrián-Lloret, V.; Metz, M.; Martínez-Abad, A.; Knutsen, S.H.; Ballance, S.; López-Rubio, A.; Martínez-Sanz, M. Valorization of alginate-extracted seaweed biomass for the development of cellulose-based packaging films. *Algal Res.* **2022**, *61*, 102576. [CrossRef]
26. Foo, K.Y.; Hameed, B.H. Insights into the modeling of adsorption isotherm systems. *Chem. Eng. J.* **2010**, *156*, 2–10. [CrossRef]
27. Cid, H.A.; Flores, M.I.; Pizarro, J.F.; Castillo, X.A.; Barros, D.E.; Moreno-Piraján, J.C.; Ortiz, C.A. Mechanisms of $Cu^{2+}$ biosorption on *Lessonia nigrescens* dead biomass: Functional groups interactions and morphological characterization. *J. Environ. Chem. Eng.* **2018**, *6*, 2696–2704. [CrossRef]
28. Davis, T.A.; Llanes, F.; Volesky, B.; Diaz-Pulido, G.; McCook, L.; Mucci, A. $^{1}$H-NMR study of Na alginates extracted from *Sargassum* spp. in relation to metal biosorption. *Appl. Biochem. Biotechnol.* **2003**, *110*, 75–90. [CrossRef]
29. Carvalho, R.P.D.; Chong, K.H.; Volesky, B. Effects of leached alginate on metal biosorption. *Biotechnol. Lett.* **1994**, *16*, 875–880. [CrossRef]
30. Fernando, I.S.; Sanjeewa, K.A.; Kim, S.Y.; Lee, J.S.; Jeon, Y.J. Reduction of heavy metal ($Pb^{2+}$) biosorption in zebrafish model using alginic acid purified from *Ecklonia cava* and two of its synthetic derivatives. *Int. J. Biol. Macromol.* **2018**, *106*, 330–337. [CrossRef]
31. Zhang, R.; Richardson, J.J.; Masters, A.F.; Yun, G.; Liang, K.; Maschmeyer, T. Effective Removal of Toxic Heavy Metal Ions from Aqueous Solution by $CaCO_3$ Microparticles. *Water Air Soil Pollut.* **2018**, *229*, 136. [CrossRef]
32. Huo, F.; Liu, Y.; Tang, Y.; Cao, Y.; Tan, C.; Yang, F.; Yang, X. Aggregation induced emission of amino-thiol capped gold nanoparticles (GNPs) through metal-amino-coordination. *Colloids Surf. B Biointerfaces* **2019**, *183*, 110335. [CrossRef]
33. Li, R.; Zhang, T.; Zhong, H.; Song, W.; Yin, X. Bioadsorbents from algae residues for heavy metal ions adsorption: Chemical modification, adsorption behavior and mechanism. *Environ. Technol.* **2020**, 1–44. [CrossRef] [PubMed]
34. Nzayisenga, J.C.; Niemi, C.; Ferro, L.; Gorzsas, A.; Gentili, F.G.; Funk, C.; Sellstedt, A. Screening Suitability of Northern Hemisphere Algal Strains for Heterotrophic Cultivation and Fatty Acid Methyl Ester Production. *Molecules* **2020**, *25*, 2107. [CrossRef]
35. Abomohra, E.F.; El-Hefnawy, M.E.; Wang, Q.; Huang, J.; Li, L.; Tang, J.; Mohammed, S. Sequential bioethanol and biogas production coupled with heavy metal removal using dry seaweeds: Towards enhanced economic feasibility. *J. Clean. Prod.* **2021**, *316*, 128341. [CrossRef]
36. Vieira, A.P.; Santana, S.A.; Bezerra, C.W.; Silva, H.A.; de Melo, J.C.; da Silva Filho, E.C.; Airoldi, C. Copper sorption from aqueous solutions and sugar cane spirits by chemically modified babassu coconut (*Orbignya speciosa*) mesocarp. *Chem. Eng. J. Lausanne* **2010**, *161*, 99–105. [CrossRef]
37. Papageorgiou, S.K.; Kouvelos, E.P.; Favvas, E.P.; Sapalidis, A.A.; Romanos, G.E.; Katsaros, F.K. Metal-carboxylate interactions in metal-alginate complexes studied with FTIR spectroscopy. *Carbohydr. Res.* **2010**, *345*, 469–473. [CrossRef]
38. Mao, S.C.; Yu, X.Y.; Shen, Y.; Zheng, K.C. Ab initio study on the H–Bonding complexes formed from phenol and a series of amides. *Chin. J. Org. Chem.* **2000**, *20*, 243–247.
39. Pereira, L.; Gheda, S.F.; Ribeiro-Claro, P.J.A. Analysis by vibrational spectroscopy of seaweed polysaccharides with potential use in food, pharmaceutical, and cosmetic industries. *Int. J. Carbohydr. Chem.* **2013**, *2013*, 7. [CrossRef]
40. Leal, D.; Matsuhiro, B.; Rossi, M.; Caruso, F. FT-IR spectra of alginic acid block fractions in three species of brown seaweeds. *Carbohydr. Res.* **2008**, *343*, 308–316. [CrossRef] [PubMed]
41. Filote, C.; Volf, I.; Santos, S.C.R.; Botelho, C.M.S. Bioadsorptive removal of Pb (II) from aqueous solution by the biorefinery waste of *Fucus spiralis*. *Sci. Total Environ.* **2018**, *648*, 1201–1209. [CrossRef] [PubMed]
42. Moirana, R.L.; Mkunda, J.; Machunda, R.; Paradelo, M.; Mtei, K. Hydroxyapatite-activated seaweed biochar for enhanced remediation of fluoride contaminated soil at various pH ranges. *Environ. Adv.* **2023**, *11*, 100329. [CrossRef]
43. Jia, C.G.; Zhang, Y.P.; Wang, H.; Ou, G.N.; Lin, J.M. Rapid biosorption and reduction removal of Cr (VI) from aqueous solution by dried seaweeds. *J. Cent. South Univ. Technol.* **2014**, *21*, 2801–2809. [CrossRef]
44. Murphy, V.; Hughes, H.; Mcloughlin, P. Comparative study of chromium biosorption by red, green and brown seaweed biomass. *Chemosphere* **2008**, *70*, 1128–1134. [CrossRef] [PubMed]
45. Gubała, D.; Taylor, N.; Harniman, R.; Rawle, J.; Hussain, H.; Robles, E.; Chen, M.; Briscoe, W.H. Structure, Nanomechanical properties, and wettability of organized erucamide layers on a polypropylene surface. *Langmuir* **2021**, *37*, 6521–6532. [CrossRef]
46. Hamdaoui, O. General analytical solution expressions for analyzing Langmuir-type kinetics of sonochemical degradation of nonvolatile organic contaminants in water. *Ultrason. Sonochemistry* **2023**, *98*, 106536. [CrossRef] [PubMed]
47. Kokalj, A. On the use of the Langmuir and other adsorption isotherms in corrosion inhibition. *Corros. Sci.* **2023**, *217*, 111112. [CrossRef]
48. Belhaj, A.F.; Elraies, K.A.; Mahmood, S.M.; Zulkifli, N.N.; Akbari, S.; Hussien, O.S. The effect of surfactant concentration, salinity, temperature, and pH on surfactant adsorption for chemical enhanced oil recovery: A review. *J. Pet. Explor. Prod. Technol.* **2019**, *10*, 125–137. [CrossRef]

49. Huangfu, C.; Yu, S.; Tong, B.; Yang, A.; Lyu, J.; Guo, X. Efficient lithium extraction from aqueous solutions by MIL-100(Fe): A study on adsorption kinetics, thermodynamics and mechanism. *Sep. Purif. Technol.* **2023**, *322*, 124365. [CrossRef]
50. Ngobeni, W.A.; Mulaba-Bafubiandi, A.F. Investigating the thermodynamics and adsorption mechanisms of alkaline gelatinised novel depressants on pyrite surface. *J. Mol. Liq.* **2023**, *384*, 122173. [CrossRef]
51. Genç-Fuhrman, H.; Mikkelsen, P.S.; Ledin, A. Simultaneous removal of As, Cd, Cr, Cu, Ni and Zn from stormwater using high-efficiency industrial sorbents: Effect of pH, contact time and humic acid. *Sci. Total Environ.* **2016**, *566–567*, 76–85. [CrossRef] [PubMed]
52. Sajib, M.; Forghani, B.; Vate, N.K.; Abdollahi, M. Combined effects of isolation temperature and pH on functionality and beany flavor of pea protein isolates for meat analogue applications. *Food Chem.* **2023**, *412*, 135585. [CrossRef]
53. Panigrahi, A.; Behera, R.K.; Mishra, L.; Kumar, S.; Dubey, P.; Dutta, S.; Sarangi, M.K. Exploring optoelectronic properties of undoped and amine-doped carbon dots: Impact of surface functionalization and pH. *Carbon* **2023**, *206*, 114–123. [CrossRef]
54. Barquilha, C.E.R.; Cossich, E.S.; Tavares, C.R.G.; Silva, E.A. Biosorption of nickel (II) and copper (II) ions by *Sargassum* sp. in nature and alginate extraction products. *Bioresour. Technol. Rep.* **2019**, *5*, 43–50. [CrossRef]
55. Zhang, R.; Richardson, J.J.; Masters, A.F.; Maschmeyer, T. Removal of $Pb^{2+}$ from water using sustainable brown seaweed phlorotannins. *Langmuir* **2022**, *38*, 8324–8333. [CrossRef]
56. Fuks, L.; Filipiuk, D.; Majdan, M. Transition metal complexes with alginate biosorbent. *J. Mol. Struct.* **2006**, *792–793*, 104–109. [CrossRef]
57. Tasić, T.; Milanković, V.; Batalović, K.; Breitenbach, S.; Unterweger, C.; Fürst, C.; Pašti, I.; Lazarević-Pašti, T. Application of viscose-based porous carbon fibers in food processing—Malathion and chlorpyrifos removal. *Foods* **2023**, *12*, 2362. [CrossRef]
58. Milanković, V.; Tasić, T.; Pejčić, M.; Pašti, I.; Lazarević-Pašti, T. Spent coffee grounds as an adsorbent for malathion and chlorpyrifos—Kinetics, thermodynamics, and eco-Neurotoxicity. *Foods* **2023**, *12*, 2397. [CrossRef]
59. Bonetto, L.R.; Ferrarini, F.; De Marco, C.; Crespo, J.S.; Guégan, R.; Giovanela, M. Removal of methyl violet 2B dye from aqueous solution using a magnetic composite as an adsorbent. *J. Water Process. Eng.* **2015**, *6*, 11–20. [CrossRef]
60. Debnath, S.; Das, R. Strong adsorption of CV dye by Ni ferrite nanoparticles for waste water purification: Fits well the pseudo second order kinetic and Freundlich isotherm model. *Ceram. Int.* **2023**, *49*, 16199–16215. [CrossRef]